Journal of Theoretical Biology 258 (2009) 537–549

Contents lists available at ScienceDirect

Journal of Theoretical Biology

journal homepage: www.elsevier.com/locate/yjtbi

Preemptive spatial competition under a reproduction–mortality constraint

Andrew Allstadt [a], Thomas Caraco [a,*], G. Korniss [b]

[a] Department of Biological Sciences, University at Albany, Albany, NY 12222, USA
[b] Department of Physics, Applied Physics, and Astronomy, Rensselaer Polytechnic Institute, 110 8th Street, Troy, NY 12180-3590, USA

ARTICLE INFO

Article history:
Received 21 August 2008
Received in revised form
23 December 2008
Accepted 17 February 2009
Available online 27 February 2009

Keywords:
Invasion analysis
Phenotypic evolution
Propagation–mortality constraint
Spatial competition

ABSTRACT

Spatially structured ecological interactions can shape selection pressures experienced by a population's different phenotypes. We study spatial competition between phenotypes subject to antagonistic pleiotropy between reproductive effort and mortality rate. The constraint we invoke reflects a previous life-history analysis; the implied dependence indicates that although propagation and mortality rates both vary, their ratio is fixed. We develop a stochastic invasion approximation predicting that phenotypes with higher propagation rates will invade an empty environment (no biotic resistance) faster, despite their higher mortality rate. However, once population density approaches demographic equilibrium, phenotypes with lower mortality are favored, despite their lower propagation rate. We conducted a set of pairwise invasion analyses by simulating an individual-based model of preemptive competition. In each case, the phenotype with the lowest mortality rate and (via antagonistic pleiotropy) the lowest propagation rate qualified as evolutionarily stable among strategies simulated. This result, for a fixed propagation to mortality ratio, suggests that a selective response to spatial competition can extend the time scale of the population's dynamics, which in turn decelerates phenotypic evolution.

1. Introduction

A number of empirical studies demonstrate neighborhood scaling of competitive effects. The count and species-identity of a sessile organism's nearest neighbors can directly impact the focal individual's growth or energy allocation (Benjamin, 1993; Cain et al., 1995; Stoll and Prati, 2001; Purves and Law, 2002; Callaway et al., 2003), indirectly influencing demographic performance. Other studies report direct effects of neighborhood composition on mortality or fecundity (Rees et al., 1996; Miriti, 2006). Interestingly, several analyses addressing spatially detailed interactions suggest that the competition is preemptive (Holway, 1998; Arenas et al., 2002; Connolly and Muko, 2003). That is, an occupied location cannot be acquired by an individual of the same or other species (other phenotype) until the current occupant's mortality opens the location (Platt and Weis, 1985; Yurkonis and Meiners, 2004; Rácz and Karsai, 2006).

Most theories for spatial competition discriminate between exclusion and coexistence of different species (Durett and Levin, 1998; Bolker et al., 2003; Snyder and Chesson, 2003). Within a population, spatially localized competitive interactions can govern the relative abundance of different genotypes (phenotypes) (Mágori et al., 2005; Wei and Krone, 2005; Caraco et al., 2006; Yasi et al., 2006; Boots and Mealor, 2007); competition between phenotypes drives the population's evolution. Our study focuses on preemptive competition between phenotypes subject to antagonistic pleiotropy between reproductive effort and mortality; we apply a basic lesson of life-history theory (Emlen, 1984; Stearns, 1992; Roff, 2002) to pairwise spatial competition.

We organize the paper as follows. First, we describe an individual-based model for locally structured competition between phenotypes; each phenotype is characterized by a propagation rate and a mortality rate. In the same section, we develop a novel quantitative prediction from a mean-field approximation to our model. Next, we constrain feasible phenotypes according to a life-history invariant analyzed by Charnov (1993); any increase in propagule-production rate (reproductive effort) implies the same proportional increase in mortality rate. In Section 3, we develop a simplified stochastic invasion model invoking local neighborhood densities to predict invasion success. The fourth section reports results drawn from simulation of the individual-based model. The combined analyses predict that selection driven by spatial competition should favor phenotypes with reduced mortality (despite their lower propagation). The Discussion summarizes and generalizes our results.

2. Spatial competition model

Our individual-based model envisions different phenotypes competing locally for the same open sites. In most cases, a

* Corresponding author. Tel.: +1 518 442 4343; fax: +1 518 442 4767.
E-mail addresses: andrew.allstadt01@albany.edu (A. Allstadt), caraco@albany.edu (T. Caraco), korniss@rpi.edu (G. Korniss).

0022-5193/$ - see front matter © 2009 Elsevier Ltd. All rights reserved.
doi:10.1016/j.jtbi.2009.02.012

resident phenotype (phenotype 1) is common initially, and an invader phenotype (phenotype 2) is initially rare. For comparison, we sometimes eliminate the resident, and the initially rare invader grows in the absence of biotic resistance.

On an $L \times L$ lattice, a site represents the minimal resources necessary to maintain a single individual. The local occupation number at site $\mathbf{x}$ is $n_i(\mathbf{x}) = 0, 1$ with $i = 1, 2$ representing the number of resident and invader-phenotype individuals, respectively. During a single time unit, one Monte Carlo step per site (MCSS), we update a total of L^2 sites in a random order. An empty site may be occupied by phenotype i through propagation from a neighboring site at rate $\alpha_i \eta_i(\mathbf{x})$, where α_i is the individual-level propagation rate for phenotype i. $\eta_i(\mathbf{x}) = (1/\delta)\Sigma_{\mathbf{x}' \in \mathrm{nn}(\mathbf{x})} n_i(\mathbf{x}')$ is the density of phenotype i in the neighborhood around site $\mathbf{x}$; $\mathrm{nn}(\mathbf{x})$ is the set of nearest neighbors of site $\mathbf{x}$, and δ is the number of sites in that neighborhood ($\delta = |\mathrm{nn}(\mathbf{x})|$).

Each phenotype also may occupy an empty site through introduction from outside the environment; introduction of individuals of each phenotype occurs at constant probabilistic rate β. An occupied site opens through density-independent mortality of the individual (Cain et al., 1995). The mortality rate for phenotype i ($i = 1, 2$) is μ_i. Summarizing transition rules for an arbitrary site $\mathbf{x}$, we have

$$0 \xrightarrow{\beta+\alpha_1\eta_1(\mathbf{x})} 1, \quad 0 \xrightarrow{\beta+\alpha_2\eta_2(\mathbf{x})} 2, \quad 1 \xrightarrow{\mu_1} 0, \quad 2 \xrightarrow{\mu_2} 0, \tag{1}$$

where 0, 1, 2 indicates that a site is open, occupied by the resident, or occupied by the invader phenotype, respectively.

Throughout, each phenotype i satisfies a persistence criterion. That is, in the absence of any introduction from outside the system, a phenotype has propagation and mortality rates assuring a non-zero probability of avoiding extinction when it grows alone (without a competing phenotype). More precisely, $\gamma_i \equiv (\alpha_i/\mu_i) > \gamma_{crit} \approx 1.649$; γ_{crit} is the critical propagation to mortality ratio. That is, if $\gamma_i < \gamma_{crit}$, then phenotype i, with certainty, grows too slowly to avert extinction even in the absence of competition, given a two-dimensional environment, $\delta = 4$ nearest neighbors, and $\beta = 0$ (Dickison and Vojta, 2005; Oborny et al., 2005; O'Malley et al., 2006a). Since μ_i^{-1} is the expected lifetime of an individual with phenotype i, γ_i is the average lifetime reproductive effort of that phenotype (Mágori et al., 2005).

During the simulations, we track the global density of each phenotype, $\rho_i(t) = (1/L^2)\sum_{\mathbf{x}} n_i(\mathbf{x}, t)$; $i = 1, 2$. To simulate an invader's growth in an empty environment, we set the resident's initial density to zero and preclude its later introduction, so that $n_1(\mathbf{x}, t) \equiv 0 \ \forall \mathbf{x}, t$.

2.1. Deterministic approximation to the spatial model

If we neglect correlations between densities at different sites (McKane and Newman, 2004), and take the naive continuum limit, the resulting deterministic (or mean-field) approximation to our individual-based spatial model leads to (O'Malley et al., 2006b; O'Malley, 2008):

$$\frac{\partial \rho_i}{\partial t} = \frac{\alpha_i}{4}(1 - \rho_1 - \rho_2)\nabla^2 \rho_i + (\beta + \alpha_i \rho_i)(1 - \rho_1 - \rho_2) - \mu_i \rho_i, \tag{2}$$

where $i = 1, 2$, and ∇^2 is the Laplace operator. In this section, we also assume homogeneous mixing, $\rho_i(\mathbf{x}, t) = \rho_i(t)$, resulting in the spatially homogeneous mean-field equations

$$\frac{d\rho_i}{dt} = (\beta + \alpha_i \rho_i)(1 - \rho_1 - \rho_2) - \mu_i \rho_i, \quad i = 1, 2. \tag{3}$$

Setting the time-derivatives in the above equations to zero,

$$0 = (\beta + \alpha_i \rho_i^*)(1 - \rho_1^* - \rho_2^*) - \mu_i \rho_i^*, \quad i = 1, 2, \tag{4}$$

which in most cases, yields a finite set of stationary densities ρ_i^*. Further, standard linear stability analysis of these fixed points (corresponding to the equilibrium densities) can help identify the stable one(s) (Appendix A).

First, since we are interested in the $\beta \ll \alpha_i, \mu_i$ regime, one can be tempted to consider $\beta = 0$ in Eq. (4). Then the locally stable, equilibrium density of phenotype i is (Appendix A)

$$\rho_i^* = \begin{cases} 0 & \text{for } \alpha_i/\mu_i < \alpha_j/\mu_j, \\ 1 - (\mu_i/\alpha_i) & \text{for } \alpha_i/\mu_i > \alpha_j/\mu_j. \end{cases} \tag{5}$$

The phenotype with the greater propagation to mortality ratio always invades and excludes the other (Neuhauser, 1992; Yu and Wilson, 2001; Shurin et al., 2004; Korniss and Caraco, 2005), and the inverse, μ_i/α_i, is the density of open sites at positive equilibrium. It is important to note that for $\alpha_1/\mu_1 \neq \alpha_2/\mu_2$, Eq. (5) is the only stable equilibrium. Further, in the context of the time evolution of the system defined by Eq. (3), this solution is reached in the $t \to \infty$ limit *independently* of the initial densities $\rho_i(0)$. Therefore, homogeneously mixed, preemptive competition precludes coexistence in the absence of repeated introduction ($\beta = 0$).

If, however, the two phenotypes have the same expected lifetime reproductive effort ($\alpha_1/\mu_1 = \alpha_2/\mu_2$), then any feasible pair (ρ_1^*, ρ_2^*) of the two types where the total density is $\rho_1^* + \rho_2^* = 1 - \gamma^{-1}$ is a neutrally stable, mean-field equilibrium ($\gamma \equiv \gamma_1 = \gamma_2$). Thus, Eq. (4) cannot determine the equilibrium densities. In the context of the time evolution of the system described by Eq. (3), this scenario simply means that the stationary densities $\rho_i(\infty)$ will depend on the initial conditions $\rho_i(0)$ when $\alpha_1/\mu_1 = \alpha_2/\mu_2$ and $\beta = 0$.

2.1.1. Extracting relevant solutions from the homogeneous mean-field equations: the $\beta \to 0$ limit

As we have seen, if $\alpha_1/\mu_1 = \alpha_2/\mu_2$, and $\beta = 0$, there is a line of fixed points ($\rho_1^* + \rho_2^* = 1 - \gamma^{-1}$) provided by Eq. (4). The actual stationary densities can be determined only by considering the time-dependent behavior of the system defined by Eq. (3), and these densities depend strongly on initial conditions. This "degeneracy" (corresponding to the line of fixed points satisfying Eq. (4)) can be removed by considering an infinitesimally small introduction rate $0 < \beta \ll 1$, i.e., considering the $\beta \to 0$ limit instead. Ecologically, this corresponds to the scenario where the introduction rate is at the level of the "noise," precisely our interest in this paper.

In this approach, one first solves Eq. (4) for a given β and *then* takes the limit of $\beta \to 0$ (Appendix B). The degeneracy is resolved, and in the small-β limit the stationary densities, *independently* of the initial conditions, are given by

$$\rho_1^* \simeq \frac{1 - \gamma^{-1}}{1 + \alpha_1/\alpha_2} + \frac{\gamma^{-1}}{1 - \gamma^{-1}} \frac{\beta}{\alpha_1} \xrightarrow{\beta \to 0} \frac{1 - \gamma^{-1}}{1 + \alpha_1/\alpha_2},$$
$$\rho_2^* \simeq \frac{1 - \gamma^{-1}}{1 + \alpha_2/\alpha_1} + \frac{\gamma^{-1}}{1 - \gamma^{-1}} \frac{\beta}{\alpha_2} \xrightarrow{\beta \to 0} \frac{1 - \gamma^{-1}}{1 + \alpha_2/\alpha_1}. \tag{6}$$

This result shows that the phenotype that attains the greater equilibrium density, the ultimately dominant type, has the smaller α_i (hence, has the smaller μ_i, since their ratio is fixed). That is, for even a very small introduction rate, the two phenotypes coexist at dynamic equilibrium, and the type with the lower demographic rates attains a higher density.

For further illustration, we show the time-dependent densities obtained by numerically integrating the homogeneous mean-field equations, Eq. (3) (Fig. 1(a)). Starting from an empty environment ($\rho_1(0) = \rho_2(0) = 0$), both phenotypes' densities initially undergo a fast growth phase. In fact, at the end of this stage, the phenotype with the higher propagation rate has attained the greater density.

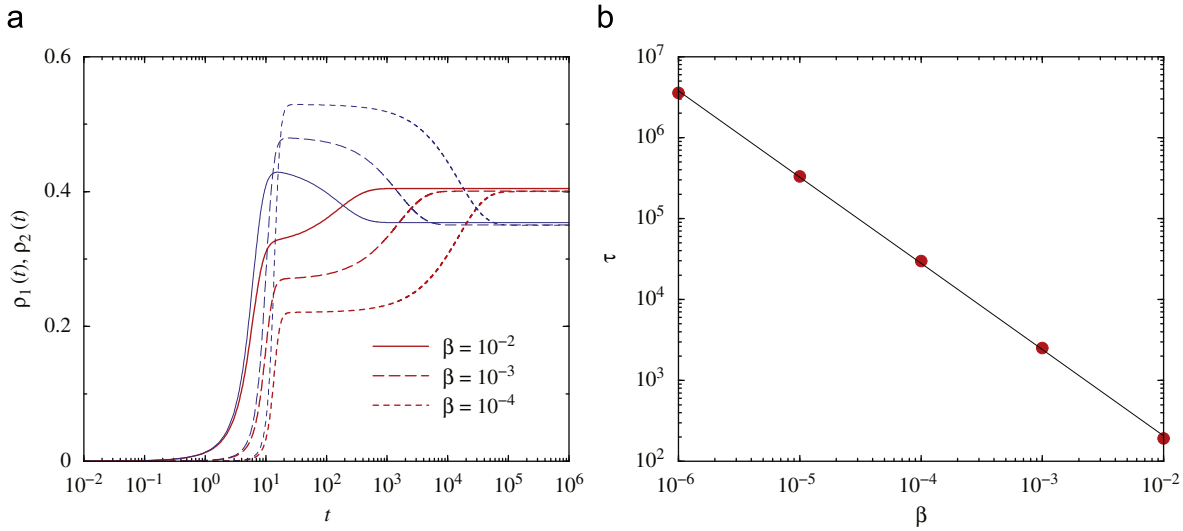

Fig. 1. (a) Numerical integration of the spatially homogeneous mean-field equations (Eq. (3)) for simultaneous invasion by the two phenotypes into an open environment ($\rho_1(0) = \rho_2(0) = 0$) for $\alpha_1 = 0.70$ (bold lines for phenotype 1), $\alpha_2 = 0.80$ (thin lines for phenotype 2), and $\gamma = 4.0$, for three values of β. Note the logarithmic scales on the horizontal axis, spanning several orders of magnitude. (b) Mean-field relaxation time (solid circles) as a function of the introduction rate for the same parameter values as in (a). τ is defined as the time where the density of the ultimately dominant phenotype first exceeds its competitor, i.e., the intersection of the corresponding time-dependent phenotype densities in (a). The straight line is the best-fit power law, corresponding to $\tau \sim \beta^{-1.06}$.

Then the system enters a very slow final equilibration stage, during which the density of the phenotype with higher propagation rate decreases, and density of the phenotype with the lower propagation rate increases. Here, one can define a characteristic time scale τ as the time when the two densities intersect and the phenotype with the lower propagation rate begins to dominate numerically. This time scale, for small β, scales approximately as $\tau \sim \beta^{-1.06}$ (Fig. 1(b)). Thus, the introduction rate strongly affects the tail of this late-stage relaxation to equilibrium. We emphasize again that as long as $\beta \neq 0$, the above stationary densities in Eq. (6) are independent of the initial condition, as illustrated in Fig. 2. Our interest in the dynamics of this seemingly special case ($\alpha_1/\mu_1 = \alpha_2/\mu_2$) is explained in the next subsection.

2.2. Propagation–mortality constraint

The spatially structured model invokes only a persistence constraint on (α_i, μ_i)-phenotypes. Life-history theory suggests consideration of a further functional constraint; an increase in propagation rate (reproductive effort) might imply a consequent increase in mortality rate (Schaffer and Rosenzweig, 1977; Emlen, 1984; Roff, 2002; Stearns, 1992). Energy or nutrient limitations can induce antagonistic pleiotropy between an individual's expenditure on reproduction and its mortality rate (Charnov, 1993; Hoyle et al., 2008). Although several spatial models analyze trade-offs between virulence and other pathogen traits (Claessen and de Roos, 1995; van Baalen, 2002; Kamo and Boots, 2004; Wei and Krone, 2005; Caraco et al., 2006), few combine functional constraints and neighborhood-scale interactions to address more general questions about demographic-trait evolution (Mágori et al., 2005; Mougi and Nishimura, 2007).

Assuming that mortality rate scales with reproductive effort, we can write $\mu \sim \alpha^{\xi}$; $\xi > 0$. Similar dependencies between demographic traits lie at the heart of life-history theory (de Mazancourt and Dieckmann, 2004; Bowers et al., 2005; Caraco and Wang, 2008; Hoyle et al., 2008). If $0 < \xi < 1$, mean lifetime reproductive effort γ, and competitive superiority in our mean-field model, increases with propagation rate α despite increased mortality. If

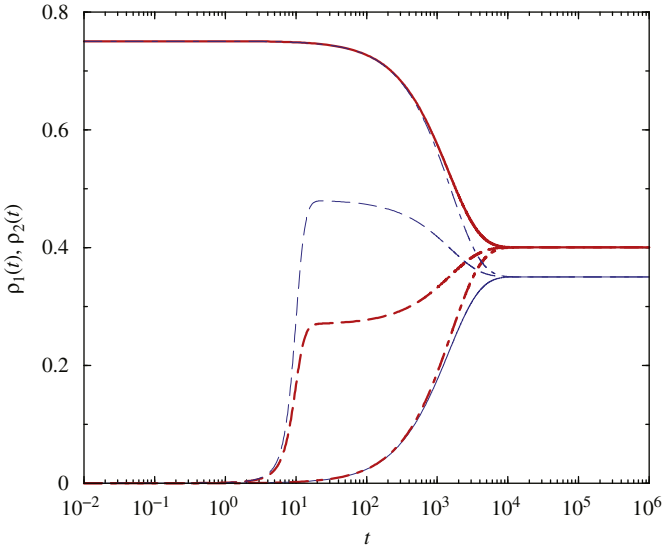

Fig. 2. Numerical integration of the spatially homogeneous mean-field equations (Eq. (3)) for different initial conditions for $\alpha_1 = 0.70$ (bold lines for phenotype 1), $\alpha_2 = 0.80$ (thin lines for phenotype 2), $\gamma = 4.0$, and $\beta = 10^{-3}$. Matching pairs of densities corresponding to initial conditions $(\rho_1(0), \rho_2(0)) = (0, 0)$, $(0, 1 - \gamma^{-1})$, and $(1 - \gamma^{-1}, 0)$ are indicated by dashed, dot-dashed, and solid lines, respectively. Note the logarithmic scales on the horizontal axis. Importantly, the phenotype densities equilibrate at the coexistence attractor given by Eq. (6) independently of initial condition.

$\xi > 1$, γ and competitive superiority now increase as α decreases, since any increase in α produces a faster increase in mortality.

However, competitive dominance under a propagation–mortality constraint may not be so simple. Charnov (1993) summarizes data on numbers of daughters per female per year (a) and annual adult mortality rate (m) for bird species differing in both body mass and niche. An invariant relationship results, perhaps reflecting an underlying functional dependence. The female clutch-size statistic a varies with adult mortality m according to $\ln a = 1.16 + \ln m$ (Charnov, 1993); the slope does not differ from unity. Since $(\ln a - \ln m)$ is constant, expected lifetime production

of daughters (a/m) is constant across species, as long as the rates do not depend strongly on age. A similar result has been inferred for a much wider set of organisms, after an allometric correction for body mass (Bell and Koufopanou, 1986).

We want to study our model's behavior when its demographic rates are restricted to the pattern in the avian trait invariance. Therefore, we set $\alpha_i/\mu_i = \gamma$, a constant across phenotypes i. The mean-field analysis, in the small-β limit, predicts the selection should favor reduced demographic rates, for fixed γ; recall Eq. (6). To investigate locally structured interactions under this constraint, we present an invasion approximation and simulation results exploring between-phenotype competition with α/μ fixed.

3. Constant α/μ and stochastic invasion

Consider neighboring sites $(\mathbf{j},\mathbf{k})$; the associated states are $[s_j(t), s_k(t)]$. A single invader (phenotype 2 individual) is introduced at site $\mathbf{j}$ at time $t=0$, producing a $[2, s_k(t)]$ block. Let $p_{0/2}$ represent the conditional probability that the site neighboring the invader is empty. $1-p_{0/2}$ is the conditional probability that an individual of the resident phenotype occupies site $\mathbf{k}$; $p_{2/2}=0$, since the just-introduced invader is rare. In general, $p_{0/2}$ should decline as the resident's density increases.

From above, the invader has mortality rate μ_2; for $t>0$, $\Pr[s_j(t)=2] = e^{-\mu_2 t}$. Mortality is simple, occurring independently of the state at any other site.

The invader may colonize neighboring site $\mathbf{k}$ via local propagation. X, a positive continuous random variable, is the waiting time until the invader occupies site $\mathbf{k}$ by propagation from site $\mathbf{j}$. We calculate its expectation $\mathrm{E}[X]$ conditioned on the invader remaining alive on $(0,X)$.

At $t=0$, $[s_j(t), s_k(t)]$ is either [2 0] or [2 1]. We associate a random residence time t_{2k} with block $[2k]$; $k=0,1$. First, assume that the initial block is [2 0]. The residence time in [2 0] is an exponential variate t_{20}. There are two feasible transitions from [2 0]; the first is:

[2 0] → [2 1], which occurs at constant probabilistic rate $(\delta-1)\eta_1\alpha_1/\delta$, where η_1 is the resident (phenotype 1) density on $\{\mathrm{nn}(\mathbf{k})-j\}$. This transition results when a resident occupying a site neighboring $\mathbf{k}$, other than $\mathbf{j}$, successfully colonizes site $\mathbf{k}$. If this transition occurs before site $\mathbf{k}$ is colonized by the invader, let t_{21} represent the exponentially distributed residence time in state [2 1]. Given state [2 1], the sole feasible transition is:

[2 1] → [2 0], which occurs at the resident's mortality rate μ_1. This transition renews the assumed initial state.

The second possible transition from [2 0] is, of course:

[2 0] → [2 2], which occurs at rate α_2/δ, and results in occupation of site $\mathbf{k}$ by the invader.

X is the total time elapsing until the invader propagates from $\mathbf{j}$ to $\mathbf{k}$. Since we first assume a [2 0] block at $t=0$, consider the conditional moment generating function:

$$M_\zeta(X|s_k(0)=0) = \mathrm{E}_0[e^{\zeta X}], \tag{7}$$

where $\mathrm{E}[\cdot]$ represents expectation. t_{20} is the waiting time until the first transition. The total transition rate from [2 0] is $(\alpha_2+[\delta-1]\alpha_1\eta_1)/\delta$, so that t_{20} has moment generating function:

$$\mathrm{E}[e^{\zeta t_{20}}] = \frac{\alpha_2+(\delta-1)\alpha_1\eta_1}{\alpha_2+(\delta-1)\alpha_1\eta_1-\delta\zeta}. \tag{8}$$

Then we can write

$$\mathrm{E}_0[e^{\zeta X}|20\to 22] = \mathrm{E}[e^{\zeta t_{20}}], \tag{9}$$

where the LHS is conditioned on propagation by the invader at the first transition. The probability that the transition at time t_{20} results in the invader occupying $\mathbf{k}$ is $\alpha_2/(\alpha_2+[\delta-1]\alpha_1\eta_1)$.

However, the initial transition from [2 0] may result in [2 1], occupation of site $\mathbf{k}$ by the resident; the probability of this transition is $[\delta-1]\alpha_1\eta_1/(\alpha_2+[\delta-1]\alpha_1\eta_1)$. Of course, the block must return, after a waiting time t_{21}, to [2 0] before the invader can occupy site $\mathbf{k}$. If the first transition results in the [2 1] block, we have

$$X = t_{20}+t_{21}+X'. \tag{10}$$

At time $(t_{20}+t_{21})$ the colonization process has recovered its state at $t=0$, as in an ordinary renewal process (Cox, 1962). Once the process has returned to the initial state, the remaining time X' has the same distribution as X (Ross, 1983). Conditioning on the resident phenotype colonizing site $\mathbf{k}$ at the first transition, we have

$$\mathrm{E}_0[e^{\zeta X}|20\to 21] = \mathrm{E}[e^{\zeta(t_{20}+t_{21}+X')}] = \mathrm{E}[e^{\zeta t_{20}}]\mathrm{E}[e^{\zeta t_{21}}]\mathrm{E}_0[e^{\zeta X}] \tag{11}$$

since the moment generating function of a sum of independent random variables is the product of the separate moment generating functions.

Since t_{21} is exponential with parameter μ_1, we have

$$\mathrm{E}_0[e^{\zeta X}|20\to 21] = \frac{\alpha_2+(\delta-1)\alpha_1\eta_1}{\alpha_2+(\delta-1)\alpha_1\eta_1-\delta\zeta}\frac{\mu_1}{\mu_1-\zeta}\mathrm{E}_0[e^{\zeta X}]. \tag{12}$$

Given $s_k(0)=0$, the conditional moment generating function of X is

$$\begin{aligned}\mathrm{E}_0[e^{\zeta X}] &= \mathrm{P}[20\to 22]\mathrm{E}_0[e^{\zeta X}|20\to 22]\\ &\quad + \mathrm{P}[20\to 21]\mathrm{E}_0[e^{\zeta X}|20\to 21].\end{aligned} \tag{13}$$

The transition probabilities are given above. Using Eqs. (9) and (12), we obtain

$$\mathrm{E}_0[e^{\zeta X}] = \frac{\alpha_2(\mu_1-\zeta)}{[\alpha_2+(\delta-1)\alpha_1\eta_1-\delta\zeta](\mu_1-\zeta)-(\delta-1)\alpha_1\eta_1\mu_1}. \tag{14}$$

Now suppose that the resident initially occupies site $\mathbf{k}$, so that $s_k(t=0)=1$, an event with probability $1-p_{0/2}$. Then the waiting time until the resident colonizes site k can be written $X = t_{21}+X'$. X' is the time elapsing following transition to block [2 0]; hence the distribution of X' has moment generating function $\mathrm{E}_0[e^{\zeta X}]$ found above. Then

$$M_\zeta(X|s_k(0)=1) = \mathrm{E}_1[e^{\zeta X}] = (\mu_1/[\mu_1-\zeta])\mathrm{E}_0[e^{\zeta X}]. \tag{15}$$

We can now write the unconditional moment generating function for the distribution of X:

$$\mathrm{E}[e^{\zeta X}] = p_{0/2}\mathrm{E}_0[e^{\zeta X}] + (1-p_{0/2})\frac{\mu_1}{\mu_1-\zeta}\mathrm{E}_0[e^{\zeta X}]. \tag{16}$$

Substituting from Eq. (14) and simplifying yields

$$\mathrm{E}[e^{\zeta X}] = \left[p_{0/2}+(1-p_{0/2})\frac{\mu_1}{\mu_1-\zeta}\right]\frac{\alpha_2(\mu_1-\zeta)}{[\alpha_2+A-\delta\zeta](\mu_1-\zeta)-A\mu_1}, \tag{17}$$

where $A=(\delta-1)\alpha_1\eta_1$.

3.1. Velocity approximation

To find the expected waiting time for invader colonization of site $\mathbf{k}$, we differentiate, since $\mathrm{E}[X] = (\mathrm{d}\mathrm{E}[e^{\zeta X}]/\mathrm{d}\zeta)_{\zeta=0}$. X need not have an exponential density, but its expectation must be finite. We designate $R = 1/\mathrm{E}[X]$ as the invader's colonization rate, in the sense that repeated observation of the colonization process has a long-run rate defined by the Elementary Renewal Theorem (Ross, 1983). The sole invader disappears at rate μ_2. Let $v = R-\mu_2$; v approximates the one-dimensional invasion velocity (rate of

progress of a sole invader) in the direction of **k**; see Ellner et al. (1998).

The colonization rate is

$$R = \frac{\alpha_2\mu_1}{\delta\mu_1 + (\delta-1)\alpha_1\eta_1 + \alpha_2(1-p_{0/2})} \tag{18}$$

R increases with α_2, μ_1, and $p_{0/2}$, as we would anticipate. R decreases as α_1 or η_1 increases, again as we anticipate. R also declines as neighborhood size δ increases, since more resident individuals compete for site **k**, though each with a lower propagation rate per site; see Korniss and Caraco (2005).

An open environment, by definition, offers no biotic resistance to invasion. When no residents impede the invader, $\eta_1 = 0$, and $p_{0/2} = 1$. For this case, X has an exponential density, and colonization simplifies to a Poisson process. Our velocity approximation becomes

$$v = (\alpha_2/\delta) - \mu_2 \tag{19}$$

which reproduces the one-dimensional velocity of the basic contact process (Ellner et al., 1998).

From the propagation–mortality constraint, $\mu_2 = \alpha_2/\gamma$ in Eq. (19), so that $\partial v/\partial\alpha_2 = (1/\delta - 1/\gamma)$. When $\gamma > \delta$, $\partial v/\partial\alpha_2 > 0$, and a phenotype with a greater propagation rate should advance faster in the absence of biotic resistance. We developed the approximation for moving "forward" along a single dimension, where the number of nearest neighbors is $\delta = 2$. The single-direction colonization rate R declines as δ increases, but in a two-dimensional environment increased opportunities for growth ($\delta = 4$) may abate this effect; see simulation results in Section 4. As long as γ/δ is not too small, Eq. (19) indicates that a phenotype with greater propagation rate will expand faster in an unoccupied environment.

In a crowded environment the resident's preemption of space resists invasion. We assume that the resident population has equilibrated at its global density ρ_1^*, so we set $\eta_1 = \rho_1^*$. For simplicity we let $p_{0/2} = 1 - \rho_1^*$, and the velocity approximation becomes

$$v = \frac{\alpha_2\mu_1}{\delta\mu_1 + (\delta-1)\alpha_1\rho_1^* + \alpha_2\rho_1^*} - \alpha_2/\gamma. \tag{20}$$

Advance of the invader requires $v > 0$. For a crowded environment, v has the sign of $[\alpha_1(1-\delta\rho_1^*) + \rho_1^*(\alpha_1 - \alpha_2) - \delta\mu_1]$. Invasive advance in a crowded environment is more likely, or proceeds faster, when $\delta\rho_1^* < 1$, and $\alpha_2 < \alpha_1$. The latter condition implies that invasion velocity v is a monotonically decreasing function of α_2. To examine this suggestion from a different perspective, note that a resident with a lower mortality rate (and lower propagation rate) will repel the invader if $(\partial v/\partial\alpha_2)_{\alpha_2=\alpha_1} < 0$; increasing the invader's α beyond the resident's diminishes the former's likelihood of invading. Taking the partial derivative, and setting $\alpha_2 = \alpha_1$, yields

$$\left(\frac{\partial v}{\partial\alpha_2}\right)_{\alpha_2=\alpha_1} = \frac{\mu_1[\delta\mu_1 + (\delta-1)\alpha_1\rho_1^*]}{[\delta\mu_1 + \delta_1\alpha_1\rho_1^*]^2} - 1/\gamma. \tag{21}$$

Recognizing that $\gamma^{-1} = \mu_1/\alpha_1$, we find that $(\partial v/\partial\alpha_2)_{\alpha_2=\alpha_1}$ has the sign of $[\delta\alpha_1\mu_1(1-2\delta\rho_1^*) + \alpha_1^2\rho_1^*(\delta - 1 - \delta^2\rho_1^*) - (\delta\mu_1)^2]$. This expression must be negative, and can permit a positive velocity, if $\delta\rho_1^* > \frac{1}{2}$. For fixed δ, ρ_1^* increases with α_i/μ_i (O'Malley et al., 2006a). Therefore, given sufficiently large γ, the analysis predicts that crowding, which intensifies preemptive competition for space, might favor a lower mortality rate, despite the lower propagation rate.

The stochastic model for a single invader's colonization or retreat (demise) in one dimension suggests the following. In an open environment, provided that the constrained vital rates imply a sufficiently high expected lifetime reproductive effort (γ), feasible phenotypes with higher α, and higher μ, values will advance faster than phenotypes with lower rates. However, once the environment becomes crowded, so that phenotypes must compete for space preemptively, low (α,μ)-phenotypes will prove competitively superior. Predictions deduced from a global analysis (Eq. (6)) and a neighborhood model (Eq. (20)) agree.

4. Spatial competition and invasion

We simulated the individual-based model on a 256×256 lattice with periodic boundaries. We kept $\delta = 4$ throughout. We divide our simulations into two experiments: invasion of an empty environment and pairwise invasion analysis.

4.1. Invading an empty environment

To simulate an initially empty environment, we set all $n_i(\mathbf{x}, t=0) = 0$. We permitted stochastic introduction of a single phenotype, or two differing phenotypes, through the course of a simulation. In both cases population growth fell in the multi-cluster regime (Korniss and Caraco, 2005; O'Malley et al., 2006a). We ran each simulation in this set for 50,000 MCSS, although the spatial system sometimes equilibrated statistically by $t \ll 50,000$.

First consider different phenotypes invading an empty environment *separately*. Fig. 3 compares global dynamics of phenotype pairs with the same expected lifetime reproductive effort γ; one member of each pair has high α and high μ, while the other has low α and low μ. The high (α,μ)-phenotype always grows more quickly than the corresponding low (α,μ)-phenotype. But each phenotype's global density equilibrates, for fixed γ, at the same level. That is, the two phenotypes (when *alone*) sequester space similarly, and global densities match predictions of ordinary pair approximation (O'Malley et al., 2006a); see figure legend. In these two-dimensional simulations, the phenotype with the greater propagation rate advanced faster in the open environment whether the common value of γ was less than ($\gamma = 2$), equal to ($\gamma = 4$), or exceeded ($\gamma = 8$) neighborhood size δ.

Next, we let pairs of phenotypes with equal γ invade an initially empty environment simultaneously; the introduction rate

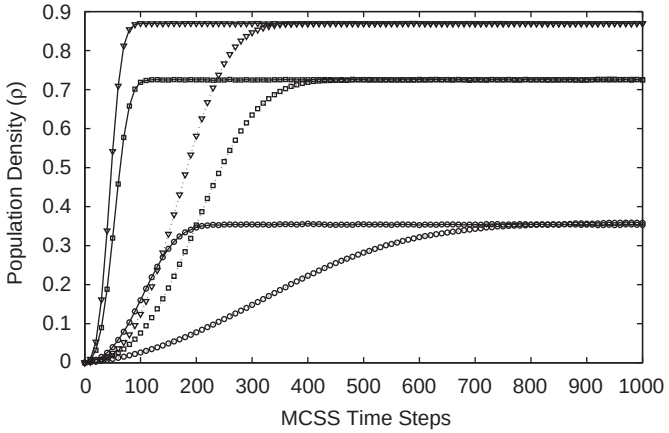

Fig. 3. A single phenotype invades an initially empty environment. Different phenotypes with same γ equilibrate at the same global density. Triangles: $\gamma = 8$; squares: $\gamma = 4$; circles: $\gamma = 2$. Within each phenotype pair solid line is high (α,μ)-phenotype, and broken line is low (α,μ)-phenotype. For each level of γ, higher $\alpha = 0.7$, and lower $\alpha = 0.1$. For $\gamma = 8$, higher $\mu = 0.0875$, and lower $\mu = 0.0125$. For $\gamma = 4$, higher $\mu = 0.175$, and lower $\mu = 0.025$. For $\gamma = 2$, higher $\mu = 0.35$, and lower $\mu = 0.05$. $\beta = 10^{-3}$. In the open environment, phenotype with higher propagation and higher mortality rate advances to equilibrium density faster. Each plot is mean of 20 simulations. Equilibrium densities best predicted by ordinary pair approximation, where $\rho^* = [4 - 1 - 4(\mu/\alpha)]/[4 - 1 - (\mu/\alpha)]$; see Eq. (22).

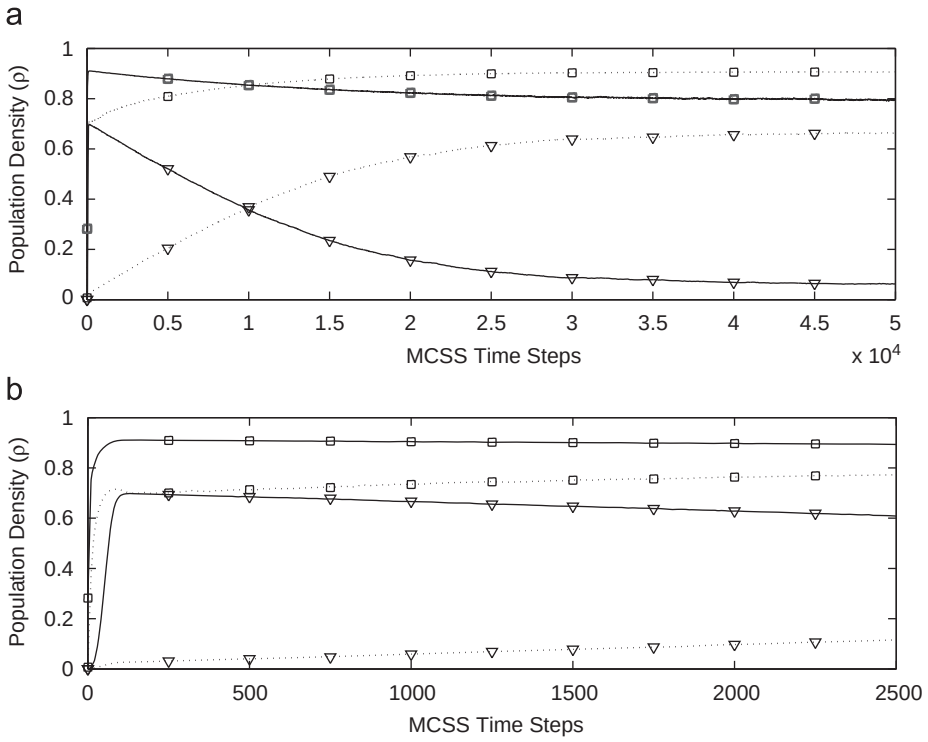

Fig. 4. Simultaneous invasion by two phenotypes, each with $\gamma = 4$. (a) 50,000 time steps plotted; each entry is mean of 20 simulations. Solid line is high (α, μ)-phenotype, where $\alpha = 0.7$, and $\mu = 0.175$. Broken line is low (α, μ)-phenotype, where $\alpha = 0.1$, and $\mu = 0.025$. Triangles indicate global densities; squares indicate conditional probability neighboring site occupied by phenotype i, given that phenotype i occupies focal site. $\beta = 10^{-3}$. Phenotype with lower demographic rates dominates numerically after first 15,000 time steps. Observed mean final densities for (low, high)-rate phenotypes are ($\rho_{low} = 0.663$, $\rho_{high} = 0.063$); coexistence equilibrium predicted by Eq. (6) is (0.656, 0.094). (b) Symbols as in (a); first 2500 time steps only. High (α, μ)-phenotype advances quickly before spatial competition increases. Both phenotypes cluster early in simulation; high (α, μ)-phenotype remains clustered as its global density declines.

was $\beta = 10^{-3}$. Fig. 4, a and b, plots the global densities for $\gamma = 4$; the pattern recurs for all α/μ simulated. The high (α, μ)-phenotype ($\alpha = 0.7, \mu = 0.175$) advances relatively quickly, almost reaching the single-phenotype global equilibrium density, Fig. 4b. But once global densities have increased sufficiently that between-phenotype competition drives the dynamics, the low (α, μ)-phenotype ($\alpha = 0.1, \mu = 0.025$) continues to advance, and the global density of the phenotype with high propagation and mortality rates declines symmetrically, Fig. 4a. By $t = 50,000$, the two phenotypes' respective densities are approximated reasonably well by the coexistence equilibrium given in Eq. (6). Fig. 4, a and b, also shows a conditional density for each phenotype. We plot the frequency at which a randomly chosen neighboring site is occupied by phenotype i, given that a focal site is occupied by that phenotype; this conditional density exceeds the global density for clustered growth (Iwasa et al., 1998; Caraco et al., 2001; Tainaka et al., 2004). Each conditional density increases rapidly; the low (α, μ)-phenotype's conditional density far exceeds its global density over the first 2500 time steps. As the high (α, μ)-phenotype declines globally, its conditional density remains high; continued introduction maintains rare clusters of the high (α, μ)-phenotype. Given sufficient time, the low (α, μ)-phenotype exhibits ecological superiority under preemptive competition. That is, its relative abundance far exceeds the frequency of the high (α, μ)-phenotype.

4.2. Pairwise invasion plots

To address spatially structured adaptive dynamics (Mágori et al., 2005; Caraco et al., 2006), we conducted pairwise invasion analyses of (α, μ)-phenotypes. We initialized the lattice with every site occupied by a resident phenotype, and simulated the individual-based dynamics for 500 time steps. This assured that the resident's global density relaxed to its single-phenotype equilibrium. Then we reset the simulation clock to $t = 0$, and began introducing an invader phenotype at probabilistic rate β (see below). Resident and invader differed in propagation and mortality rates, but the ratio γ was identical. We also introduced individuals of the resident phenotype at the same stochastic rate. Since the competing phenotypes had the same expected lifetime reproductive success, symmetry of introduction focused the invasion analysis on consequences of between-phenotype differences in demographic rates. In parallel, this procedure allowed us to compare simulation results to coexistence-equilibrium densities predicted by Eq. (6).

Ordinarily, we define successful invasion as advance from rarity. However, many ecologists interested in exotic species replace the dynamics-based concept of invasion, preferring definitions combining biogeographic, physiological, environmental, and/or demographic processes. Richardson et al. (2000) organize some of the terminology. Therefore, we used a criterion that requires both advance from rarity and significant impact on the resident. Specifically, we recorded a successful invasion if the initially rare invader phenotype reduced the resident's global density to less than one-half ρ_i^* (defined below) before 50,000 time steps had elapsed. Otherwise, we recorded a failed invasion. For each resident–invader pair, we repeated the simulation 20 times and estimated the probability of successful invasion.

When only a single phenotype advances to equilibrium in simulation, ordinary pair approximation (Keeling et al., 1997; Iwasa et al., 1998; Caraco et al., 2001) accurately predicts the global density; see the legend for Fig. 3. O'Malley et al. (2006a) analyze the ordinary pair approximation to our stochastic spatial

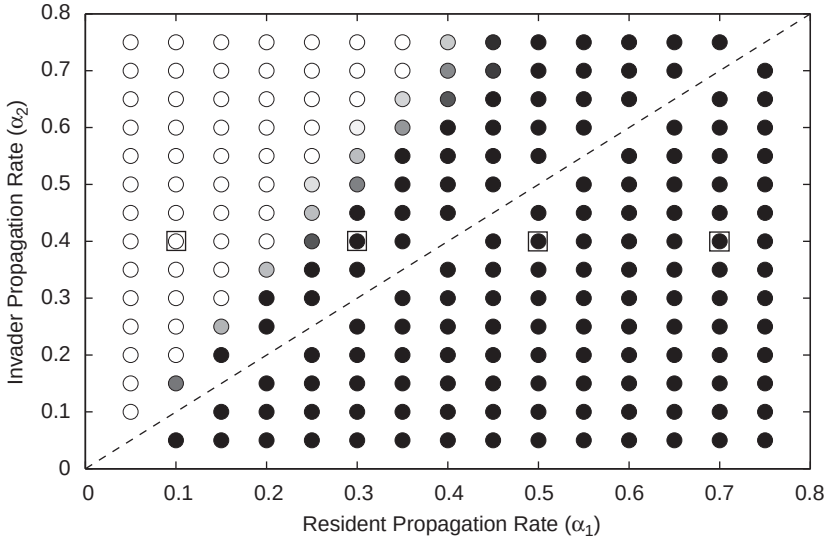

Fig. 5. Pairwise invasion plot for $\gamma = 2$. Each entry indicates frequency at which invader phenotype, on ordinate, successfully invaded resident phenotype, on abscissa. White—no successful invasion in 20 simulations; invasion frequency increases as gray darkens; black–successful invasion in each of 20 simulations. Global dynamics for the four entries in squares plotted in Fig. 8.

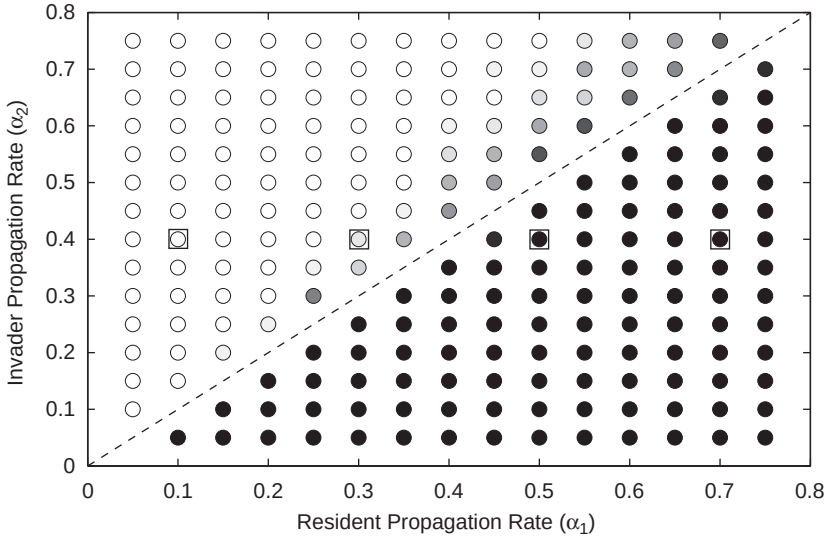

Fig. 6. Invasion plot for $\gamma = 4$. Symbols as defined in legend for Fig. 5. Global dynamics for entries in squares plotted in Fig. 9.

model. For $\beta = 0$, the positive equilibrium, global density of phenotype i is

$$\rho_i^* = \frac{\delta - 1 - \delta(\mu_i/\alpha_i)}{\delta - 1 - (\mu_i/\alpha_i)}. \tag{22}$$

Hence ρ_i^* should be the global density of any resident phenotype before an invader is introduced. Our criterion for successful invasion then implies that an invader must advance sufficiently to reduce the resident's global density below $\rho_i^*/2$ at least once during simulation.

Fig. 5 shows the pairwise invasion plot (PIP) for $\gamma = 2$. Below the diagonal, the invader is the low (α, μ)-phenotype; above the diagonal, the opposite is true. Greater probabilities of successful invasion are indicated by darker entries in the PIP. A lower (α, μ)-phenotype always invades a higher (α, μ)-phenotype successfully. Near the diagonal, where the differences in the phenotypes' demographic rates are very small, higher (α, μ) can often invade lower (α, μ), but this effect disappears as the resident's demographic rates decrease. The phenotype with the lowest mortality rate ($\mu = 0.025$) and lowest propagation rate ($\alpha = 0.05$) successfully invaded all other phenotypes simulated, and no other phenotype simulated could ever invade it. Hence, the phenotype combining the lowest propagation and mortality rates fulfills the definition of an evolutionarily stable strategy (ESS); see Geritz et al. (1998). When mean lifetime reproductive effort is held constant, any phenotype with greater expected longevity than a resident should invade and exclude that resident.

Fig. 6 displays the PIP for $\gamma = 4$, and Fig. 7 shows the PIP for $\gamma = 8$. Patterns and interpretation are clear. Phenotypes with lower mortality rates (hence lower propagation rates) will be favored through pairwise preemptive competition for space. In each plot the phenotype combining the lowest mortality and propagation rates qualifies as an ESS among the competing types simulated.

The pairwise invasion analyses exhibit some quantitative variation as γ increases from 2 to 8. The overall frequency of successful invasion decreases as expected lifetime reproductive effort γ increases. Of course, as γ increases the global frequency of

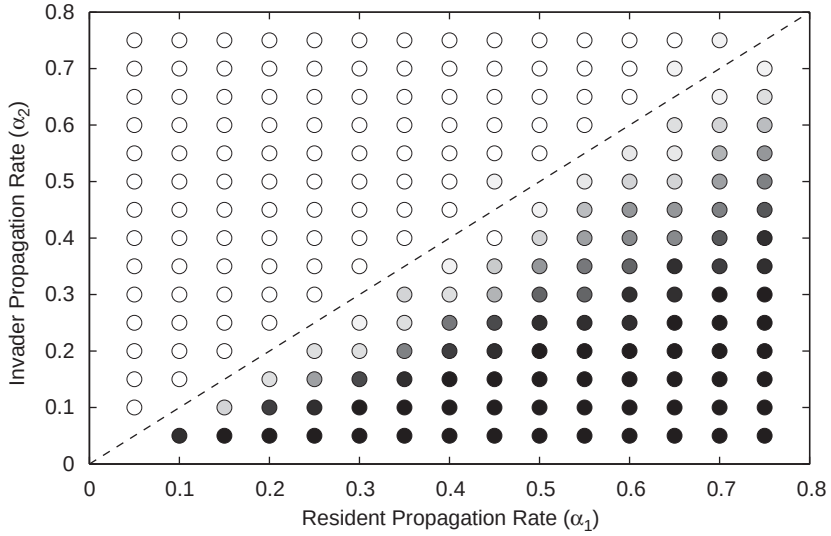

Fig. 7. Invasion plot for $\gamma = 8$. Symbols as defined in legend for Fig. 5.

empty sites $(1 - \rho_i^*)$, where introductions occur, decreases. An increased number of introduction events might increase the likelihood of mutual invasibility. Therefore, we repeated the invasion analyses after adjusting the introduction rate β as a function of γ so that the expected number of introduction events per unit time was the same at each level of γ. The resulting invasion plots were nearly identical to Figs. 5–7.

The decline in frequency of invasion with increasing γ may be due partly to our definition of invasion. A successful invader's advance from rarity reduces the resident to $\frac{1}{2}$ its single-phenotype equilibrium density under pair approximation at least once during 50,000 time steps. A lesser γ_i implies a reduced ρ_i^* and consequently a smaller "distance" from the invasion threshold. An important question asks whether or not decline in resident density results from an (approximately) equal increase in the density of the competing invader. Not surprisingly, this is the case. Fig. 8 shows time-dependent global densities of residents and invaders from the four phenotype pairs marked in Fig. 5, where $\gamma = 2$. The figure also plots the conditional neighborhood densities defined for Fig. 4. We show means of 20 simulations. In each plot the invader has $\alpha = 0.4$ and $\mu = 0.2$; the introduction rate is $\beta = 10^{-3}$.

In Fig. 8a the resident has the low (α, μ)-phenotype, and invasion never succeeds. After 10,000 time steps the invader's density, maintained by repeated introduction, has equilibrated, and the invader's presence is mirrored in the decline of the competitively dominant resident to coexistence densities. So, the invader persists but its presence does not impact the resident significantly. In Fig. 8b the resident again has the lower mortality and propagation rates, but the difference between phenotypes is small. Each phenotype's global density has equilibrated by $t = 10,000$. The resident's density, in any given simulation, declines enough to fulfil our definition of a successful competitive invasion. In Fig. 8c and d, the invader now has the low (α, μ)-phenotype, successfully invades in every simulation, and reaches numerical superiority by 10,000 time steps. The conditional densities show clear spatial clustering of each phenotype; conditional densities are less sensitive to differences between phenotypes than are global densities. Overall, successful invasion leads to coexistence of phenotypes. The summed densities of the two phenotypes equal, on average, the same total density in each case. The invader's global density increases as the difference between its mortality rate and the resident's mortality rate decreases from positive to negative. Invader growth drives the resident's decline. Whether resident or invader, the lower (α, μ)-phenotype possesses a competitive advantage, reflected in its numerical superiority.

Fig. 9 shows global densities of resident and invader populations from the four phenotype pairs marked in Fig. 6, where $\gamma = 4$. In each plot the invader has $\alpha = 0.4$ and $\mu = 0.1$; the introduction rate remains $\beta = 10^{-3}$. Compared to the dynamics in Fig. 6, the propagation rates are the same, but the mortality rate has been halved. In Fig. 9a the resident's lower mortality rate implies that invasion never succeeds. In Fig. 9b, mortality rates are closer, and invasion succeeds in 25% of simulations. In Fig. 9c and d, the invader has the low (α, μ)-phenotype, and invasion always succeeds. As in Fig. 8 the low (α, μ)-phenotype always attains the greater equilibrium density. The increased γ, compared to Fig. 8, increases equilibrium densities, and the reduced mortality rate more than doubles the time for the system to reach equilibrium coexistence.

To complete the results, consider the final densities from each plot in Figs. 8 and 9. First, Fig. 10 shows the difference in final densities (invader minus resident) as a function of the difference in mortality rates of the phenotypes (resident minus invader). The phenotype with the lower mortality rate attains the greater final density in each case. The response to the mortality-rate difference is greater among phenotype pairs with $\gamma = 4$, where total population densities are greater than for $\gamma = 2$.

Fig. 11 compares observed and predicted frequencies of the invader phenotype for both $\gamma = 2$ and 4. Frequencies are of two types: global invader density, ρ_2^* predicted by Eq. 6, and relative frequency within the population (i.e., phenotype frequency $\rho_2^*/[\rho_1^* + \rho_2^*]$). Observed global densities are, on average, less than predicted. But predicted relative frequencies, on average, match observations of the coexisting phenotypes quite well.

5. Discussion

For sessile organisms, ecological interactions commonly are restricted to a local neighborhood (Rees et al., 1996; Stoll and Prati, 2001; Miriti, 2006). These spatially structured, individual-level processes can combine with distance-limited propagule dispersal to generate a landscape of growing and contracting clusters (Cain et al., 1995; Schwinning and

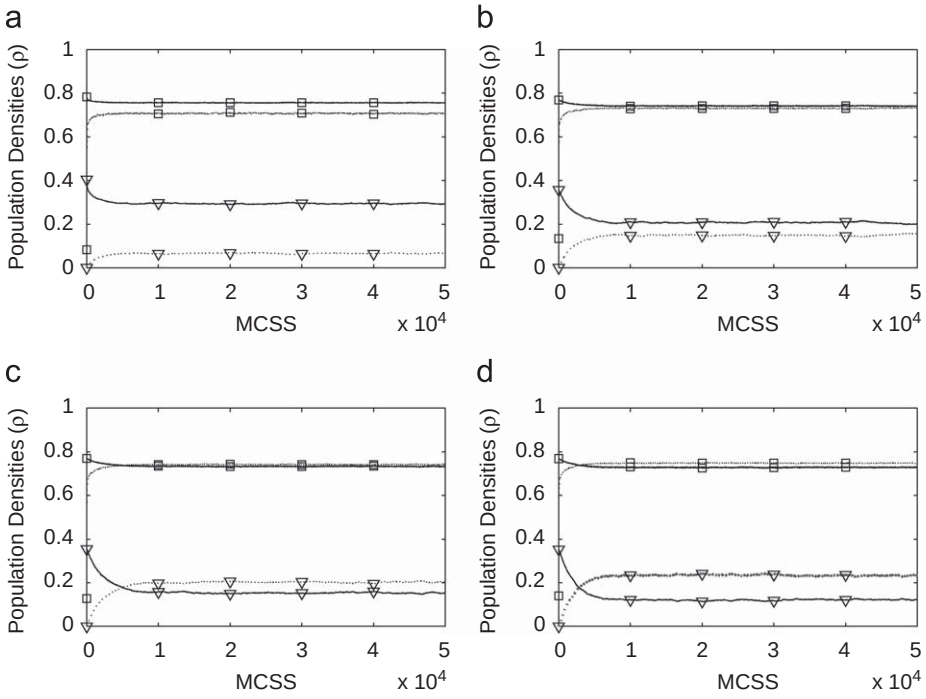

Fig. 8. Invasion dynamics, $\gamma = 2$. Global and local dynamics of phenotype pairs marked by squares in Fig. 5. In each plot invader has $\alpha = 0.4$, and $\mu = 0.2$. Invader dynamics indicated by broken line; triangle is invader's global density, and square is conditional frequency of invader given an invader at neighboring site. Solid line follows resident's global (triangles) and conditional (squares) densities. Introduction of each phenotype occurs at probabilistic rate $\beta = 10^{-3}$. Each entry is mean of 20 simulations. (a) Resident has low (α, μ)-phenotype ($\alpha = 0.1, \mu = 0.05$). Between-phenotype difference large enough that successful invasion never occurs. (b) Resident has low (α, μ)-phenotype ($\alpha = 0.3, \mu = 0.15$). Between-phenotype difference small enough that invasion succeeds; resident maintains higher global density. (c) Resident has high (α, μ)-phenotype ($\alpha = 0.5, \mu = 0.25$). Invasion always succeeds, and invader has greater global density. (d) Resident has $\alpha = 0.7$ and $\mu = 0.35$. Invader has much lower mortality rate; invasion always succeeds, and invader has significantly greater global density. Clustering of both phenotypes remains less variable than do the global densities.

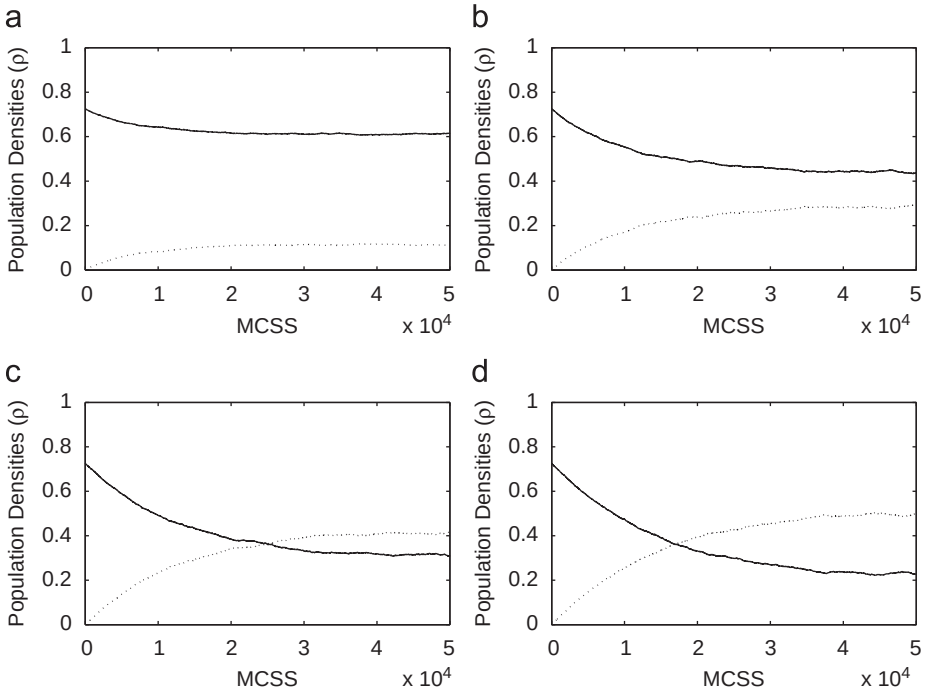

Fig. 9. Invasion dynamics, $\gamma = 4$. Global densities of phenotype pairs marked by squares in Fig. 6. In each plot invader has $\alpha = 0.4$, and $\mu = 0.1$. Invader dynamics indicated by broken line; solid line is resident's density. Each phenotype introduced at rate $\beta = 10^{-3}$. Each entry is mean of 20 simulations. (a) Resident has low (α, μ)-phenotype ($\alpha = 0.1, \mu = 0.025$); successful invasion does not occur in any of 20 simulations. (b) Resident has low (α, μ)-phenotype ($\alpha = 0.3, \mu = 0.075$), but rates closer. Invasion successful in 25% of simulations. (c) and (d) Invader now has low (α, μ)-phenotype; resident has ($\alpha = 0.5, \mu = 0.125$) in (c), and ($\alpha = 0.7, \mu = 0.175$) in (d). Invasion succeeds in each simulation, and invader's equilibrium density exceeds resident's density. Comparing these results to preceding figure shows that doubling expected lifetime reproductive effort (via halved mortality) approximately doubles each species' equilibrium density, and the reduced mortality rates increase time the system requires to reach equilibrium. Note that consistent failure of invasion in plot a reflects our criterion. Invader density advances from rarity to coexistence level that exceeds introduction-driven fluctuations, but resident's density does not decline sufficiently to meet our definition of successful invasion.

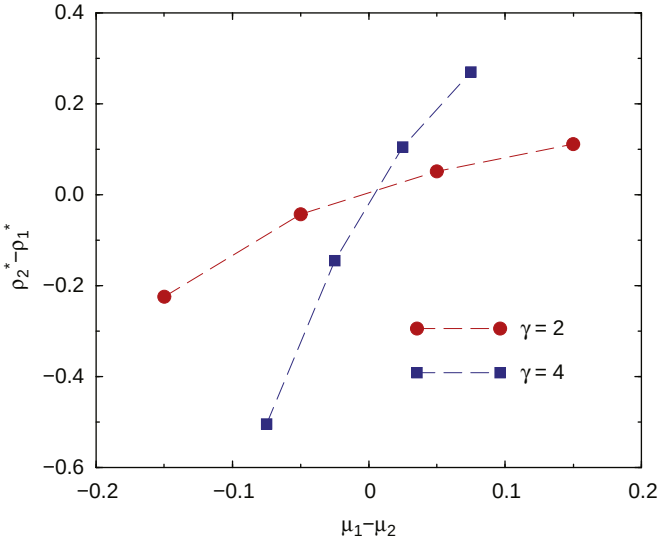

Fig. 10. Difference in equilibrium density depends on difference in mortality rates. We calculated mean densities over last 50 time steps, assuring statistical equilibrium, for each phenotype's dynamics plotted in Figs. 8(a–d) and 9(a–d). We show the invader's mean density minus the resident's mean density as a function of the resident's mortality rate minus the invader's mortality rate. Circles: $\gamma = 2$; squares: $\gamma = 4$. The phenotype with the lesser mortality rate has the greater equilibrium density; that is, invader density exceeds resident density when the resident has the greater mortality rate. Response to mortality-rate difference greater as γ increases.

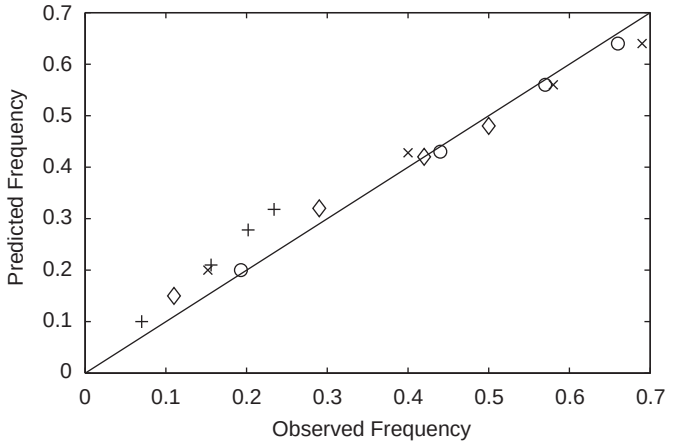

Fig. 11. Observed vs predicted invader frequencies at coexistence equilibrium. Plus sign: invader global densities for $\gamma = 2$. Circle: invader relative abundances for $\gamma = 2$. Diamond: invader global densities for $\gamma = 4$. X: invader relative abundance for $\gamma = 4$. Predictions employ Eq. (6); observations calculated from terminal densities in Figs. 8 and 9.

Parsons, 1996; Gandhi et al., 1999; Tainaka et al., 2004; Korniss and Caraco, 2005). Conspecific interactions predominate within sufficiently large clusters, and between-species (or between-phenotype) interactions occur more often at the interface between clusters (Silvertown et al., 1994; O'Malley et al., 2005; Allstadt et al., 2007). A better understanding of relationships among neighborhood-scale processes, the spatial dynamics of endogenous clustering, and persistence or extinction of populations remains a challenge to evolutionary ecology (Avrami, 1941; van Baalen and Rand, 1998; Wilson, 1998; Pascual and Levin, 1999; Dieckmann et al., 2000; Parsons et al., 2001; O'Malley et al., 2006a).

Studies by Mágori et al. (2005) and by Wei and Krone (2005) include questions similar to those we ask. Detailed comparison is encumbered by differing definitions of invasion/coexistence. Mágori et al. (2005) analyze two populations competing on a 100×100 lattice. They initialized simulations by occupying each site with an individual chosen with equal probability from the two populations. They averaged each population's global density over the second half of each simulation, and considered a population extinct if its mean density was less than 10% of the more numerous population's mean density. Extensive simulations by Mágori et al. (2005) include a two-type contact process with nearest-neighbor propagation, density-independent mortality, and no introduction during simulation; see their second figure. When their two populations have different local demographic rates, but the same propagation/mortality ratio, Mágori et al. (2005) find coexistence in that neither type fulfils their extinction criterion.

Wei and Krone (2005) analyze an expanding cluster of disease by simulating an SIR epidemic on a lattice. Infection and recovery occur as a contact process, but a recovered site does not return to susceptibility. Wei and Krone (2005) place a mutant pathogen at or beyond the perimeter of a cluster of a wild-type infection. The mutant's infection and recovery rates (propagation and mortality in our model) differ from the wild-type's rates. The mutant invades successfully if at least 90 lattice sites are mutant-occupied 250 time units after introduction. Wei and Krone (2005) find that the frequency of successful invasion increases as the mutant's propagation rate increases, even if accompanied by increased mortality. Given the mutant's position at introduction, its advance is similar to our invasion of an "empty" environment, where high propagation can be advantageous until population density, and consequent spatial competition, favor reduced mortality.

Our preemptive competition model conforms to a 2-type contact process with immigration. If one phenotype has a greater expected lifetime reproductive effort (α/μ), it will be favored selectively (Neuhauser, 1992; Mágori et al., 2005; O'Malley et al., 2005). However, this study (motivated by life-history theory) examines phenotypes that have the same α/μ value, but differ in characteristic longevity. Our approximate analyses and detailed simulations compared invasion of an empty environment (no resident) with introduction of a rare phenotype to an environment crowded with individuals of a resident phenotype. An unoccupied environment favors faster growth, i.e., greater $(\alpha_i - \mu_i)$ when $(\alpha_i/\mu_i) = \gamma$. Cluster expansion in the absence of a resident implies that mortalities can be replaced quickly, given the lack of biotic resistance along a cluster's perimeter. But this is a transient effect when rapid growth crowds the environment, and between-phenotype competition ensues. Crowded environments, contrastingly, favor low morality. A superior competitor must maintain sites for a much longer time, waiting for mortality to open a site and provide an opportunity to reproduce. In every case (Figs. 8 and 9) the low (α, μ)-phenotype reaches numerical superiority, given sufficiently long simulation time.

The pairwise invasion analyses suggest an evolutionary trait-replacement series, where selection continues to favor increased longevity and reduced reproductive effort per unit time, given a fixed mean lifetime reproductive effort. An immediate ecological consequence would be an increase in the time scale of the population dynamics. In particular, the expected time elapsing until a competitively superior invader's global density first surpasses the resident's density will grow. Equivalently, the pace of between-phenotype selective evolution would decline. Evolving to an effectively "frozen" adaptive dynamics, and phenotypic stasis, is perhaps unlikely. Any alteration in the functional dependence between propagation and mortality, reshaping the tradeoff (Schaffer, 1974; Hoyle et al., 2008), would unlock potential for further life-history evolution.

Our analytical and computational results depend on both the assumed preemptive competition for sites and, as just noted, the assumption that α/μ is fixed. Specificity of the assumptions limits predictions of our models accordingly; competing phenotypes need not have the same mean lifetime reproductive effort. But our theoretical comparison of growth in "open" vs "closed" environments offers a framework for integrating certain seemingly disparate observations. In the study of breeding systems the "ecological constraints hypothesis" asserts that maturing offspring should remain with their parents as helpers, rather than accepting costs of dispersal and territory establishment, if environmental crowding leaves few breeding sites open (Brown, 1987; Koenig et al., 1992). Pruett-Jones and Lewis (1990) found that young male wrens (*Malurus cyaneus*) remained helpers at their parents' nest when most breeding territories were occupied. But upon removal of breeding males, helper males quickly dispersed to newly opened sites and began establishing their own breeding territories (Pruett-Jones and Lewis, 1990). A crowded environment apparently favored lesser reproductive effort, while the open environment favored greater reproductive effort, despite the increased costs.

We also can liken our results to traits favored in early vs late spatial succession. Higher propagation rate may offer short-term advantage during rapid increase in population densities. But lower mortality, increasing persistence (Keeling, 2000), might be more important later on when community densities equilibrate, and competition increases. Finally, our model's open sites can serve as a metaphor for hosts susceptible to pathogen infection (Grassberger, 1983; Wei and Krone, 2005). When infections have plentiful access to susceptibles, an open environment, higher transmission rates could be favored, even at the cost of rapid decay of infectious particles. But when susceptible density declines, persistent infectious particles (spores) might be favored, to promote host contacts, even if the transmission probability per susceptible encounter were reduced through antagonistic pleiotropy (Caraco and Wang, 2008).

Recall that Eq. (2) presents the mean-field approximation to our spatial competition model. "Mean-field" implies that we neglect random fluctuations, and consequent spatial correlations, among sites, while the equations retain spatial dependence (McKane and Newman, 2004). Next, we made the further assumption of homogeneous mixing. This assumption relaxes any spatial dependence; each site interacts with all others equally, leading to the spatially homogeneous mean-field equations (3). Dropping random fluctuations from the model and dropping spatial dependence are distinct actions; see Hiebeler (1997) or McKane and Newman (2004).

After applying the assumption of homogeneous mixing to our mean-field model, we found that treatment of the (small) introduction rate β qualitatively alters the dynamics of competitors with the same mean lifetime reproductive effort. If we set $\beta = 0$, and then let the system equilibrate, the initial conditions govern the two competitors' densities at (neutrally stable) equilibrium. If, however, we let the dynamics, Eq. (3), equilibrate and then take the limit as $\beta \to 0$, we find a single, locally stable, positive equilibrium node, given by Eq. (6), for any feasible initial condition. The latter treatment better approximates our simulation procedures and, more importantly, demonstrates that rare introduction events, at the level of "noise," assure coexistence of the phenotypes. At the resulting equilibrium, the competitor with the lower mortality (hence, lower propagation) rate will be more abundant.

Our pairwise invasion analyses verified that preemptive spatial competition can favor reduced mortality at the expense of propagation, when life histories are constrained by fixed γ. Summarily, we have congruence among the mean-field analysis equation (6), the local stochastic invasion model equation (20), and our individual-based results.

Acknowledgments

The National Science Foundation supported this research through Grant DEB-0342689. We thank Z. Toroczkai for providing us with a generic code for the numerical integration of the mean-field equations. We appreciate the reviewers comments; they offered both careful corrections and insightful interpretation. We also thank L. O'Malley, J.A. Newman, I.-N. Wang and G. Robinson for discussion.

Appendix A. Mean-field fixed points and their stability for $\beta = 0$

$\rho_1(t)$ is the resident phenotype's global density, and $\rho_2(t)$ is the invader's global density. Setting the introduction rate $\beta = 0$ for each phenotype, the spatially homogeneous mean-field equations, Eq. (3) of the text, become

$$\dot{\rho_1} = (\alpha_1 - \mu_1)\rho_1 - \alpha_1\rho_1^2 - \alpha_1\rho_1\rho_2, \tag{A.1}$$

$$\dot{\rho_2} = (\alpha_2 - \mu_2)\rho_2 - \alpha_2\rho_2^2 - \alpha_2\rho_1\rho_2, \tag{A.2}$$

$\alpha_i > \mu_i$ for each phenotype, precluding stability of mutual extinction ($\rho_1^* = 0$, $\rho_2^* = 0$). The Jacobian is

$$J = \begin{bmatrix} \alpha_1 - \mu_1 - 2\alpha_1\rho_1 - \alpha_1\rho_2 & -\alpha_1\rho_1 \\ -\alpha_2\rho_2 & \alpha_2 - \mu_2 - 2\alpha_2\rho_2 - \alpha_2\rho_1 \end{bmatrix}. \tag{A.3}$$

Consider the resident phenotype at its equilibrium global density and the invader rare. Evaluating the Jacobian at ($\rho_1^* = 1 - \mu_1/\alpha_1$, $\rho_2^* = 0$), the roots of the characteristic equation $\det[J - \lambda I] = 0$ are $\lambda_a = \mu_1 - \alpha_1$ and $\lambda_b = \mu_1(\alpha_2/\alpha_1) - \mu_2$. The resident repels invasion if both roots are negative. From above, $\mu_1 < \alpha_1$ is required for feasibility of the resident's positive equilibrium density. From the second root, the invader fails to advance when rare if $\alpha_1/\mu_1 > \alpha_2/\mu_2$. Otherwise, phenotype 2 successfully invades the initial resident if

$$\alpha_2/\mu_2 = \gamma_2 > \gamma_1 = \alpha_1/\mu_1. \tag{A.4}$$

If inequality (A.4) holds, a parallel argument shows that phenotype 1 cannot invade phenotype 2 when the latter rests at its equilibrium global density ($\rho_2^* = 1 - \mu_2/\alpha_2$). Furthermore, inequality (A.4) precludes equilibrium coexistence, and phenotype 2 competitively excludes phenotype 1 when $\gamma_2 > \gamma_1$. However, if $\gamma_1 = \gamma_2 = \gamma$, linear combinations of the phenotypes, constrained by the total global density, $\rho_1^* + \rho_2^* = 1 - \gamma^{-1}$, are neutrally stable (Mágori et al., 2005).

Appendix B. Solution of the homogeneous mean-field equations for $\alpha_1/\mu_1 = \alpha_2/\mu_2$ and $\beta \neq 0$

Under the reproduction–mortality constraint $\gamma = \alpha_1/\mu_1 = \alpha_2/\mu_2$, for arbitrary β, the mean-field equations for the fixed points (Eq. (4)) read

$$\begin{aligned} &(\beta/\alpha_1 + \rho_1)(1 - \rho_1 - \rho_2) - \gamma^{-1}\rho_1 = 0, \\ &(\beta/\alpha_2 + \rho_2)(1 - \rho_1 - \rho_2) - \gamma^{-1}\rho_2 = 0, \end{aligned} \tag{B.1}$$

where $(\rho_1 + \rho_2) < 1$. By introducing a new variable Δ for convenience, through $\rho_1 + \rho_2 = 1 - \gamma^{-1} + \Delta$, we can recast the above system of equations as

$$\begin{aligned} &(\beta/\alpha_1 + \rho_1)(\gamma^{-1} - \Delta) - \gamma^{-1}\rho_1 = 0, \\ &(\beta/\alpha_2 + \rho_2)(\gamma^{-1} - \Delta) - \gamma^{-1}\rho_2 = 0, \\ &\rho_1 + \rho_2 - (1 - \gamma^{-1}) = \Delta, \end{aligned} \tag{B.2}$$

which can be further simplified,

$$\beta(\gamma^{-1}-\Delta)=\alpha_1\rho_1\Delta,$$
$$\beta(\gamma^{-1}-\Delta)=\alpha_2\rho_2\Delta,$$
$$\rho_1+\rho_2-(1-\gamma^{-1})=\Delta. \tag{B.3}$$

The first two equations above immediately imply that (for $\beta\neq 0$) $\alpha_1\rho_1=\alpha_2\rho_2$, i.e., the greater equilibrium density of the dominant phenotype implies that it has the smaller α_i. It is also instructive to solve the above system of equations explicitly. After eliminating, e.g., ρ_2 and Δ, following elementary algebra, one finds a quadratic equation for ρ_1

$$\left(1+\frac{\alpha_1}{\alpha_2}\right)\rho_1^2+\left[\frac{\beta}{\alpha_1}\left(1+\frac{\alpha_1}{\alpha_2}\right)-(1-\gamma^{-1})\right]\rho_1-\frac{\beta}{\alpha_1}=0. \tag{B.4}$$

The above equation has a single positive root

$$\rho_1^*=\frac{1}{2\left(1+\frac{\alpha_1}{\alpha_2}\right)}\left\{(1-\gamma^{-1})-\frac{\beta}{\alpha_1}\left(1+\frac{\alpha_1}{\alpha_2}\right)+\sqrt{\left[\frac{\beta}{\alpha_1}\left(1+\frac{\alpha_1}{\alpha_2}\right)-(1-\gamma^{-1})\right]^2+4\frac{\beta}{\alpha_1}\left(1+\frac{\alpha_1}{\alpha_2}\right)}\right\}. \tag{B.5}$$

The analogous expression for ρ_2 has the same form as above, except for interchanging α_1 with α_2. While substituting $\beta=0$ into Eq. (B.5) immediately yields the desired densities, it is insightful to expand the above expression as a Taylor series, which also provides the corrections to the $\beta\to 0$ limit. Up to first order in β, one finds

$$\rho_1^*=\frac{1-\gamma^{-1}}{1+\alpha_1/\alpha_2}+\frac{\gamma^{-1}}{1-\gamma^{-1}}\frac{\beta}{\alpha_1}+\mathcal{O}(\beta^2),$$
$$\rho_2^*=\frac{1-\gamma^{-1}}{1+\alpha_2/\alpha_1}+\frac{\gamma^{-1}}{1-\gamma^{-1}}\frac{\beta}{\alpha_2}+\mathcal{O}(\beta^2). \tag{B.6}$$

Thus, through infinitesimally small positive β, the densities approach the limits

$$\lim_{\beta\to 0}\rho_1^*=\frac{1-\gamma^{-1}}{1+\alpha_1/\alpha_2},$$
$$\lim_{\beta\to 0}\rho_2^*=\frac{1-\gamma^{-1}}{1+\alpha_2/\alpha_1}. \tag{B.7}$$

References

Allstadt, A., Caraco, T., Korniss, G., 2007. Ecological invasion: spatial clustering and the critical radius. Evol. Ecol. Res. 9, 1–20.

Arenas, F., Viejo, R.M., Fernández, C., 2002. Density-dependent regulation in an invasive seaweed: responses at plant and modular levels. J. Ecol. 90, 820–829.

Avrami, M., 1941. Geometry and dynamics of populations. Philos. Sci. 8, 115–132.

Bell, G., Koufopanou, V., 1986. The cost of reproduction. In: Dawkins, R., Ridley, M. (Eds.), Oxford Surveys in Evolutionary Biology, vol. 3. Oxford University Press, Oxford, UK, pp. 83–131.

Benjamin, L.R., 1993. Experimental discrimination between contrasting models of neighborhood competition. J. Ecol. 81, 417–423.

Bolker, B.M., Pacala, S.W., Neuhauser, C., 2003. Spatial dynamics in model plant communities: What do we really know? Am. Nat. 162, 135–148.

Boots, M., Mealor, M., 2007. Local interactions select for lower pathogen infectivity. Science 315, 1284–1286.

Bowers, R.G., Hoyle, A., White, A., Boots, M., 2005. The geometric theory of adaptive evolution: trade-off and invasion plots. J. Theor. Biol. 233, 363–377.

Brown, J.L., 1987. Helping and Communal Breeding in Birds. Princeton University Press, Princeton, NJ.

Cain, M.L., Pacala, S.W., Silander, J.A., Fortin, M.-J., 1995. Neighborhood models of clonal growth in the white clover *Trifolium repens*. Am. Nat. 145, 888–917.

Callaway, R.M., Pennings, S.C., Richards, C.L., 2003. Phenotypic plasticity and interactions among plants. Ecology 84, 1115–1128.

Caraco, T., Duryea, M., Glavanakov, S., Maniatty, W., Szymanski, B.K., 2001. Host spatial heterogeneity and the spread of vector-borne disease. Theor. Popul. Biol. 59, 185–206.

Caraco, T., Glavanakov, S., Li, S., Maniatty, W., Szymanski, B.K., 2006. Spatially structured superinfection and the evolution of disease virulence. Theor. Popul. Biol. 69, 367–384.

Caraco, T., Wang, I.-N., 2008. Free-living pathogens: life history constraints and strain competition. J. Theor. Biol. 250, 569–579.

Charnov, E.L., 1993. Life History Invariants: Some Explorations of Symmetry in Evolutionary Ecology. Oxford University Press, Oxford, UK.

Claessen, D., de Roos, A.M., 1995. Evolution of virulence in a host–pathogen system with local pathogen transmission. Oikos 74, 401–413.

Connolly, S.R., Muko, S., 2003. Space preemption, size-dependent competition, and the coexistence of clonal growth forms. Ecology 84, 2979–2988.

Cox, D.R., 1962. Renewal Theory. Methuen & Co., London.

de Mazancourt, C., Dieckmann, U., 2004. Trade-off geometries and frequency-dependent selection. Am. Nat. 164, 765–778.

Dickison, M., Vojta, T., 2005. Monte Carlo simulations of the smeared phase transition in a contact process with extended defects. J. Phys. A Math Gen. 38, 1188–1208.

Dieckmann, U., Law, R., Metz, J.A.J. (Eds.), 2000. The Geometry of Ecological Interactions: Simplifying Spatial Complexity. Cambridge University Press, Cambridge, UK.

Durrett, R., Levin, S., 1998. Spatial aspects of interspecific competition. Theor. Popul. Biol. 53, 30–43.

Ellner, S.P., Sasaki, A., Haraguchi, Y., Matsuda, H., 1998. Speed of invasion in lattice population models: pair-edge approximation. J. Math. Biol. 36, 469–484.

Emlen, J.M., 1984. Population Biology. Macmillan Publishing, New York, NY.

Gandhi, A., Levin, S., Orszag, S., 1999. Nucleation and relaxation from meta-stability in spatial ecological models. J. Theor. Biol. 200, 121–146.

Geritz, S.A.H., Kisdi, E., Meszéna, G., Metz, J.A.J., 1998. Evolutionarily singular strategies and the adaptive growth and branching of the evolutionary tree. Evol. Ecol. 12, 35–57.

Grassberger, P., 1983. On the critical behavior of the general epidemic process and dynamical percolation. Math. Biosci. 63, 157–172.

Hiebeler, D., 1997. Stochastic spatial models: from simulations to mean field and local structure approximations. J. Theor. Biol. 187, 307–319.

Holway, D.A., 1998. Factors governing rate of invasion: a natural experiment using Argentine ants. Oecologia 115, 206–212.

Hoyle, A., Bowers, R.G., White, A., Boots, M., 2008. The influence of trade-off shape on evolutionary behaviour in classical ecological scenarios. J. Theor. Biol. 250, 498–511.

Iwasa, Y., Nakamuru, M., Levin, S.A., 1998. Allelopathy of bacteria in a lattice population: competition between colicin-sensitive and colicin-producing strains. Evol. Ecol. 12, 785–802.

Kamo, M., Boots, M., 2004. The curse of the pharaoh in space: free-living infectious stages and the evolution of virulence in spatially explicit populations. J. Theor. Biol. 231, 435–441.

Keeling, M., 2000. Evolutionary trade-offs at two time scales: competition versus persistence. Proc. R. Soc. London B 267, 385–391.

Keeling, M.J., Rand, D.A., Morris, A.J., 1997. Correlation models for childhood epidemics. Proc. R. Soc. London B 264, 1149–1156.

Koenig, W., Pitelka, F.A., Carmen, W.J., Mumme, R.L., Stanback, M.T., 1992. The evolution of delayed dispersal in cooperative breeders. Quart. Rev. Biol. 67, 111–150.

Korniss, G., Caraco, T., 2005. Spatial dynamics of invasion: the geometry of introduced species. J. Theor. Biol. 233, 137–150.

Mágori, K., Szabó, P., Mizera, F., Meszéna, G., 2005. Adaptive dynamics on a lattice: role of spatiality in competition, co-existence and evolutionary branching. Evol. Ecol. Res. 7, 1–21.

McKane, A.J., Newman, T.J., 2004. Stochastic models in population biology and their deterministic analogues. Phys. Rev. E 70 (041902), 19.

Miriti, M., 2006. Ontogenetic shift from facilitation to competition in a desert shrub. J. Ecol. 94, 973–979.

Mougi, A., Nishimura, K., 2007. Evolution of life-history traits collapses competitive coexistence. J. Theor. Biol. 248, 552–559.

Neuhauser, C., 1992. Ergodic theorems for the multitype contact process. Probab. Theory Rel. Fields 91, 467–506.

Oborny, B., Meszéna, G., Szabó, G., 2005. Dynamics of populations on the verge of extinction. Oikos 109, 291–296.

O'Malley, L., 2008. The advance of an advantageous allele: nucleation, front propagation, and seasonal effects. Ph.D. Thesis, Rensselaer Polytechnic Institute, Troy, NY.

O'Malley, L., Allstadt, A., Korniss, G., Caraco, T., 2005. Nucleation and global time scales in ecological invasion under preemptive competition. In: Stocks, N.G., Abbott, D., Morse, R.P. (Eds.), Fluctuations and Noise in Biological, Biophysical, and Biomedical Systems III. Proceedings of SPIE, vol. 5841. SPIE, Bellingham, WA, pp. 117–124.

O'Malley, L., Basham, J., Yasi, J.A., Korniss, G., Allstadt, A., Caraco, T., 2006a. Invasive advance of an advantageous mutation: nucleation theory. Theor. Popul. Biol. 70, 464–478.

O'Malley, L., Kozma, B., Korniss, G., Rácz, Z., Caraco, T., 2006b. Fisher waves and front propagation in a two-species invasion model with preemptive competition. Phys. Rev. E 74 (041116), 7.

Parsons, A.J., Schwinning, S., Carrère, P., 2001. Plant growth functions and possible spatial and temporal scaling errors in models of herbivory. Grass Forage Sci. 56, 21–34.

Pascual, M., Levin, S.A., 1999. From individuals to population densities: searching for the intermediate scale of nontrivial determinism. Ecology 80, 2225–2236.

Platt, W.J., Weis, I.M., 1985. An experimental study of competition among fugitive prairie plants. Ecology 66, 708–720.
Pruett-Jones, S., Lewis, M., 1990. Sex ratio and habitat limitation promote delayed dispersal in superb fairy wrens. Nature 348, 541–542.
Purves, D.W., Law, R., 2002. Experimental derivation of functions relating growth of *Arabidopsis thaliana* to neighborhood and distance. J. Ecol. 80, 882–894.
Rácz, E.V.P., Karsai, J., 2006. The effect of initial pattern on competitive exclusion. Commun. Ecol. 7, 23–33.
Rees, M., Grubb, P.J., Kelly, D., 1996. Quantifying the impact of competition and spatial heterogeneity on the structure and dynamics of a four-species guild of winter annuals. Am. Nat. 147, 1–32.
Richardson, D.M., Pyšek, P., Rejmánek, M., Barbour, M.G., Panetta, F.D., West, C.J., 2000. Naturalization and invasion of alien plants: concepts and definitions. Div. Distr. 6, 93–107.
Roff, D.A., 2002. Life History Evolution. Sinauer Associates, Sunderland, MA.
Ross, S.M., 1983. Stochastic Processes. Wiley, New York.
Schaffer, W.M., 1974. Optimal reproductive effort in fluctuating environments. Am. Nat. 108, 783–790.
Schaffer, W.M., Rosenzweig, M.L., 1977. Selection for optimal life histories. II. Multiple equilibria and the evolution of alternate reproductive strategies. Ecology 58, 60–72.
Schwinning, S., Parsons, A.J., 1996. A spatially explicit population model of stoloniferous N-fixing legumes in mixed pasture with grass. J. Ecol. 84, 815–826.
Shurin, J.B., Amarasekare, P., Chase, J.M., Holt, R.D., Hoopes, M.F., Leibold, M.A., 2004. Alternative stable states and regional community structure. J. Theor. Biol. 227, 359–368.
Silvertown, J., Lines, C.E.M., Dale, M.P., 1994. Spatial competition between grasses—rates of mutual invasion between four species and the interaction with grazing. J. Ecol. 82, 31–38.
Snyder, R., Chesson, P., 2003. Local dispersal can facilitate coexistence in the presence of permanent spatial heterogeneity. Ecol. Lett. 6, 301–309.
Stearns, S.C., 1992. The Evolution of Life Histories. Oxford University Press, Oxford, UK.
Stoll, P., Prati, D., 2001. Intraspecific aggregation alters competitive interactions in experimental plant communities. Ecology 82, 319–327.
Tainaka, K., Kushida, M., Itoh, Y., Yoshimura, J., 2004. Interspecific segregation in a lattice ecosystem with intraspecific competition. J. Phys. Soc. Japan 73, 2914–2915.
van Baalen, M., 2002. Contact networks and the evolution of virulence. In: Dieckmann, U., Metz, J.A.J., Sabelis, M.W., Sigmund, K., Law, R., Metz, H. (Eds.), Adaptive Dynamics of Infectious Diseases: In Pursuit of Virulence Management. Cambridge University Press, Cambridge, UK, pp. 85–103.
van Baalen, M., Rand, D.A., 1998. The unit of selection in viscous populations and the evolution of altruism. J. Theor. Biol. 193, 631–648.
Wei, W., Krone, S.W., 2005. Spatial invasion by a mutant pathogen. J. Theor. Biol. 236, 335–348.
Wilson, W., 1998. Resolving discrepancies between deterministic population models and individual-based simulations. Am. Nat. 151, 116–134.
Yasi, J., Korniss, G., Caraco, T., 2006. Invasive allele spread under preemptive competition. In: Landau, D.P., Lewis, S.P., Schüttler, H.-B. (Eds.), Computer Simulation Studies in Condensed Matter Physics XVIII. Springer, Heidelberg, Germany, pp. 165–169.
Yu, D.W., Wilson, H.B., 2001. The competition-colonization trade-off is dead: long live the competition-colonization trade-off. Am. Nat. 158, 49–63.
Yurkonis, K.A., Meiners, S.J., 2004. Invasion impacts local species turnover in a successional system. Ecol. Lett. 4, 764–769.